Evaluating effective reaction rates of kinetically driven solutes in large-scale, anisotropic media: human health risk implications

ERICA R. SIIRILA & REED M. MAXWELL

Dept. of Geology and Geological Engineering, Colorado School of Mines, 1500 Illinois St., Golden, Colorado 80401, USA

esiirila@mymail.mines.edu

Abstract The role of high and low hydraulic conductivity regions in heterogeneous, stratified flow fields and the subsequent effect of rate dependent geochemical reactions are investigated. Human health risk (cancer) is used as an endpoint for comparison via a two-stage nested Monte Carlo scheme, explicitly considering joint uncertainty and variability. Parameter interplay is investigated using stochastic ensembles. This study identifies the effect of geo-hydrologic conditions on solute equilibrium and the effect of preferential flow pathways and mixing at the field and local scales for varying degrees of stratification. Results show effective reaction rates of kinetic ensembles are dissimilar from equilibrium ensembles with local dispersion, resulting in an additive tailing effect of the solute plume, a retarded peak time, and an increased risk. Uncertainty in risk is also controlled by these factors. We demonstrate that a higher associated uncertainty of risk in stratified domains is linked to higher aquifer connectivity and less macrodispersion.

Key words cancer risk; kinetic sorption; local dispersion; stochastic Monte Carlo; CO_2 leakage; arsenic

INTRODUCTION

Contradictory to field and laboratory observations showing non-ideal, or kinetic behaviour of reactive solutes (e.g. Pickens *et al*., 1981; Roberts *et al*., 1986), contaminant transport studies are often modelled using a linear equilibrium assumption (LEA), and may therefore prove problematic for accurately quantifying human health risk. Correctly identifying point values of the contaminant plume (i.e. at a well) is imperative for accurately calculating human health risk because groundwater concentrations are often directly used as exposure values to assess risk. The importance of fundamental groundwater flow and transport processes in risk assessment has been demonstrated in multiple studies (Andričević *et al*., 1994, 1996; Maxwell *et al*., 1999; Smalley *et al*., 2000; Hassan *et al*., 2001; Benekos *et al*., 2003, 2007; Tartakovsky, 2007; Bolster & Tartakovsky, 2008; de Barros & Rubin, 2008; Maxwell *et al*., 2008; Bolster *et al*., 2009; de Barros *et al*., 2009; Siirila *et al*., 2012). Most recently, the influence of a contaminant's sorptive capacity was found to be a controlling factor in determining if risk exceeded United States Environmental Protection Agency (EPA) remediation action levels (RAL) (Siirila *et al*., 2012). Under an exposure duration of 30 years, differing degrees of instantaneous equilibrium sorption (referred to here as the local equilibrium assumption, LEA) yielded a nonlinear probability of an individual incurring cancer over a lifetime and/or experiencing an adverse health effect, where values of predicted risk varied by over an order of magnitude. This finding warrants further analysis of the assumption of LEA in risk assessment.

In the present study, a theoretical case study is used to simulate an example contamination scenario (i.e. CO_2 leakage in Carbon Capture and Storage, CCS) involving mobilized arsenic. Arsenic is a worldwide contaminant of concern in groundwater resources and is furthermore of importance due to its high cancer and non-cancer adverse health effects. Both the validity and predictability of LEA is investigated by stochastically simulating ensembles of both linear and kinetic sorption scenarios that should theoretically retard the solute equally if equilibrium is an appropriate assumption. An investigation of potential inter-play (positive or negative feedbacks) between multiple hydro-geologic parameters is conducted for both kinetic and LEA ensembles. In particular, the effect of preferential flow pathways and solute mixing on the field-scale (macrodispersion) and sub-grid (local dispersion) is examined for varying degrees of stratified,

heterogeneous flow fields. The stratified aquifer is of interest because inter-connected pathways are much more prevalent, where channelling of solutes through areas of higher hydraulic conductivity effectively decrease the overall effect of macrodispersion (Siirila *et al*., 2012). Finally, carcinogenic human health risk is used as an endpoint of comparison by utilizing the methodology developed by Siirila *et al*. (2012). Risk is calculated for a population of potentially exposed individual using a nested Monte Carlo approach, explicitly considering uncertainty in environmental parameters and variability in individual physiological and exposure parameters.

METHODOLOGY

Following the framework of Siirila *et al*. (2012), far-field groundwater flow and solute transport is modelled stochastically to account for uncertainty in groundwater flow paths. A complete set of the governing equations for flow, transport, and for human health risk are described in Siirila *et al*. (2012) and are not shown here for brevity.

Hydrologic flow field, heterogeneity, and solute transport

Uncertainty in hydrologic flow and subsurface properties is accounted for by the use of a stochastic Monte Carlo scheme where multiple realizations of equally probable heterogeneous subsurface domains are simulated, all honouring the same global statistics. An isotropic exponential correlation model is used to define spatial correlation of hydraulic conductivity K (m/d) via a separation distance (ξ) (m) and correlation lengths in the horizontal and vertical directions (λ_h, λ_v, respectively) (m):

$$R^e_{ff}(\xi) = \sigma^2 \exp^{-\xi/\lambda} \quad (1)$$

In this study, the magnitude of λ_h is used to describe the degree of aquifer stratification and is a principal parameter investigated in the sensitivity analysis of the case study. The degree of stratification is discussed in terms of the anisotropy ratio, $\varepsilon = \lambda_v / \lambda_h$ (–). Far-field aquifer flow is simulated using the parallel, three-dimensional groundwater model ParFlow (Ashby & Falgout, 1996; Jones & Woodward, 2001; Kollet & Maxwell, 2006) and spatially correlated random fields of K are internally generated in ParFlow using the turning bands algorithm (Tompson *et al*., 1989).

Realizations of flow fields are linked to a solute transport model to simulate plume migration from a fixed pulse source. Sensitivity to hydraulic properties is explored by generating multiple ensembles of varying hydraulic properties and analysing the statistical outcome of an endpoint measured in the solute transport model (i.e. concentration at a well). Solute transport is simulated using the Lagrangian particle tracking model SLIM-FAST (Maxwell & Kastenberg, 1999; Maxwell *et al*., 2007; Maxwell, 2010). Non-reactive (i.e. tracer), LEA, and first-order kinetic particle simulations are conducted. LEA simulations utilize the partition coefficient (K_D) (L kg^{-1}), defined as the slope of sorption isotherm. Kinetic simulations utilize time dependent forward (k_f) (L d^{-1}) and reverse (k_r) (kg d^{-1}) rates with an equivalent ratio to the partition coefficient $K_D = k_f/k_r$. All sorption parameters (K_D, k_f, k_r) are constant in space and time. Here the retardation (R) (–) of the solute is a direct relationship with K_D for LEA simulations and the ratio (k_f/k_r) for kinetic simulations, where $R_{LEA} = (1 + \rho_b K_D/\theta)$ and $R_{kin} = [1 + (\rho_b k_f/k_r\theta)]$. Local, or pore-scale dispersion (PSD) has also been linked to sensitivity in higher order moments (i.e. point flux and concentration variances) (Dagan & Fiori, 1997; Fiori *et al*., 2002; Fiorotto & Caroni, 2002; Bellin *et al*., 2004). This increase in dispersion is quantified in terms of displacement by the non-dimensional Péclet number (Pe) and simplified through the dispersivity relationship ($D_L = \alpha_L v_x$) as $Pe = (v_x\lambda/D_L) = (\lambda_h/\alpha_L$ (–).

Peak concentration distributions, effective retardations, connectivity indicator

To quantify the effects of each parameter adjusted in the sensitivity analysis (i.e. ε, Pe, sorption scenario) the peak time (t_{pk} (d)) and peak concentration normalized with the initial concentration

(C_{pk}/C_0 (–)) at which the maximum mass arrives at the well is calculated (for each well, per realization). A cumulative distribution function (CDF) where each point represents a well in a realization of the ensemble is then compared. For each sorption scenario, effective retardation is expressed relative to t_{pk} and C_{pk}/C_0 of the corresponding tracer simulation of that realization:

$$R_{eff,LEA} = \frac{t_{pk,LEA}}{t_{pk,tracer}}, \quad R_{eff,kin} = \frac{t_{pk,kin}}{t_{pk,tracer}} \tag{2}$$

This essentially uses the conservative tracer simulations as a control by holding the parameters ε and *Pe* constant and isolating the effect of the sorption scenario alone. Equation (2) is based on the results of the numerical simulations and describes the effective retardation of the overall plume. Due to the relationship between the ratio k_f/k_r and K_D (see definition above), if LEA is an appropriate assumption, $R_{eff,LEA}$ is equivalent to $R_{eff,kin}$, regardless of the hydrologic domain or the transport parameters.

Lastly, the effect of channelling through preferential flow paths is investigated calculating the connectivity indicator, *CI* (–). As described by Knudby & Carrera (2005), the shape of the breakthrough curve (higher order moments), can be used to relate the degree of connectivity within an aquifer. Here we define *CI* as the ratio of the time at which 5% of particle mass is present at the well (t_5) (d), and the time at which 50% of the particle mass is present at the well (t_{50}) (d) via $CI = t_{50}/t_5$. A higher *CI* value signifies a breakthrough curve skewed towards earlier arrival times and significant tailing. A higher *CI* value indicates high channelling when compared to lower *CI* values (Knudby & Carrera, 2005). Parameter inputs are listed in Table 1.

Table 1 Flow and transport parameter values.

Parameter	Value	Units
Domain size (x, y, z)	~ (4000 × 1000 × 100)	(m)
Cell discretization (x, y, z)	(3.0 × 3.0 × 0.3)	(m)
Number of cells (x, y, z)	(1333 × 333 × 333)	–
Location of source (x, y, z)	(500.0, 500.0, 30.0), 300 000 particles	(m)
Geometric mean, st. dev. of ln(K)	$K_{G,ln(K)} = 52$, $\sigma_{ln(K)} = 1.9$	(m d^{-1}), (–)
Porosity	$\theta = 0.33$	–
Well pumping rates	$Q = 500$	(m^3 d^{-1})
Well locations (4)	$x_w = 3500$, $z_w = 75$, ($y_w = 800$, 600, 400 200)	(m)
Anisotropy ratios		
$\varepsilon = 0.1$ (–)	$\lambda_h = 15.0$, $\lambda_v = 1.5$	(m)
$\varepsilon = 0.006$ (–)	$\lambda_h = 250.0$, $\lambda_v = 1.5$	(m)
Sorption scenarios		
LEA, partition coefficient	$K_D = 25$	(L kg^{-1})
Kin1, forward and reverse rates	$k_f = 2.88$, $k_r = 0.115$	(L d^{-1})
Local dispersion scenarios		
$Pe = \infty$ (–)	$\alpha_L = 0.0$, $\alpha_T = 0.0$	(m)
$Pe = 1.5 \times 10^4$ (–)	For $\lambda_h = 15.0$: $\alpha_L = 0.001$, $\alpha_T = 0.0001$	(m)
$Pe = 2.5 \times 10^5$ (–)	For $\lambda_h = 250.0$: $\alpha_L = 0.001$, $\alpha_T = 0.0001$	(m)

RESULTS

Peak concentration distributions

For each of the four wells, C_{pk}/C_0 is calculated using elution curves for each. Figure 1 shows the inner well ($y_w = 600$ (m), 400 (m)) ensemble CDFs of C_{pk}/C_0 for a continuous source term. Varying ε (see key for each sub-plot in Fig. 1), and *Pe* (Fig. 1 (a) *versus* (b)) are compared. LEA distributions are shown as solid lines whereas *Kin1* distributions are shown in dashed lines.

General trends include: (1) an increase in the C_{pk}/C_0 distribution variance with a decrease in ε and (2) an increase in the C_{pk}/C_0 distribution variance with an increase in *Pe*. These results are consistent with the findings of Siirila *et al*. (2012). Changes in macrodispersion can be used to explain the greater variance in CDF distribution with lower ε. In the more stratified domain (ε = 0.006 (–)), the aquifer is subject to lower solute spreading through channelling in interconnected *K* zones. This channelling results in a binary distribution of the solute arriving at the well where elution water is either (1) clean, and the connected zone does not follow a pathway connecting from the source to the well or (2) highly concentrated, and a connected zone between the source to the well exists. This behaviour can be thought of as a "hit or miss" probability. A quantitative discussion of results regarding channelling is presented below. Lastly, the increase in distribution variance attributed to finite *Pe* is related to the imposed cell-based dispersion or mixing within the model. While it is expected that the inclusion of local dispersion will increase distribution variance, it should be noted that the cell-based mixing imposed for each cell is minute, equal to 1.0 (mm) in the longitudinal direction and 0.1 (mm) in the transverse direction (see Table 1). The increase in C_{pk}/C_0 distribution variance (imposed by an increase in *Pe* and a decrease in ε) is physically relatable to the probability of pumping non-contaminated water from the well. For example, the percentage of clean groundwater withdrawal from a stratified aquifer varies between approximately 20 and 90% whereas the less stratified aquifers are always pumping contaminated water.

The left panel of Fig. 2 shows ensemble CDFs of infinite *Pe* whereas the right panel of Fig. 1 shows ensemble CDFs of finite *Pe* (i.e. $Pe = 1.5 \times 10^4$ for $\varepsilon = 0.1$ and $Pe = 2.5 \times 10^5$ for $\varepsilon = 0.006$). The magnitude of C_{pk}/C_0 values are also approximately two orders of magnitude less for ensemble CDFs of the pulse source term in comparison to the continuous source term. *Kin1* ensembles (dashed lines) are clearly distinguishable from LEA ensembles (solid lines), suggesting LEA is not an appropriate assumption given these hydrologic conditions, where for all scenarios (Fig. 1(a)–(f)) LEA ensembles over-estimate the magnitude of C_{pk}/C_0 values and do not dramatically affect the variance of the distribution. The lesser kinetic C_{pk}/C_0 values are attributed to delayed mass breakthrough at the well (i.e. a longer tailing effect). A disparity between finite *Pe* (Fig. 1(b)) and for infinite *Pe* (Fig. 1(a)) is also apparent, especially for *Kin1* ensembles. This is attributed to an additive effect between the time dependence in kinetic sorption and local dispersion, also observed in ensembles utilizing the continuous source term. These results show interdependence between kinetic sorption and local dispersion not previously documented. Here the induced cell-based mixing creates particle jumps from interconnected high *K* regions into regions of low *K* and *vice versa*.

We speculate that the effect of the time dependence associated with kinetic sorption into and out of solution is magnified, yielding solute behaviour unlike that of equilibrium simulations. Key findings in the additive process involving kinetic sorption and PSD include: (1) particle retardation similar to LEA in low *K* zones where low *v* regimes are conducive to equilibrium conditions, (2) lower particle retardation in high *K* zones via less reaction time in high *v* regimes, (3) shorter particle displacement in low *K* zones and longer particle displacements in high *K* zones, and (4) a higher frequency of t_{Disp} in LEA scenarios compared to kinetic scenarios.

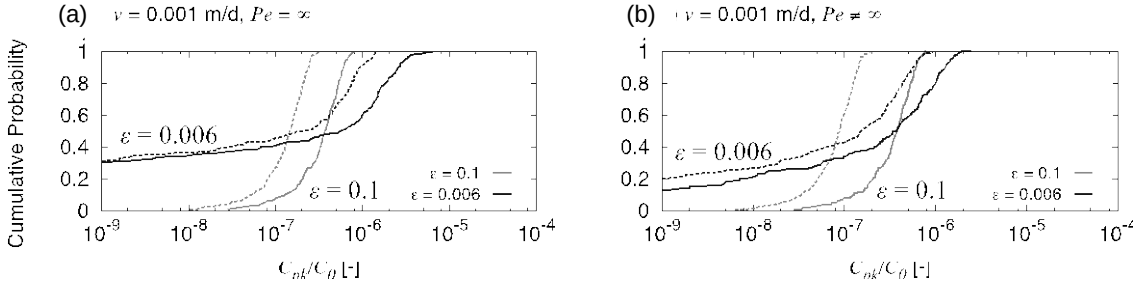

Fig. 1 CDFs of inner well normalized peak concentrations for infinite *Pe* (a) and finite *Pe* (b).

Effective retardation factor

In addition to comparing normalized peak concentrations, corresponding peak times (t_{pk}) are also analysed. t_{pk} for each sorption scenario ($t_{pk,LEA}$ and $t_{pk,Kin1}$) are normalized by t_{pk} time of the tracer ($t_{pk,tracer}$, equation (2)), effectively factoring out the effects of heterogeneity to analyse the sole effect of differences in *Kin1* and LEA ensembles. Figure 2 shows a scatter plot (12 ensembles, 200 realizations each) of effective kinetic retardations ($R_{eff,Kin1}$) *versus* normalized peak tracer concentrations ($C_{pk}/C_{pk,tracer}$) with infinite *Pe* (a) and finite *Pe* (b). To demonstrate the behaviour of the majority of particles, values corresponding to breakthrough mass greater than or equal to 5% of the source mass are shown. The vertical bar at R_{eff} = 26 (–) corresponds to the expected solute retardation if equilibrium is an appropriate assumption.

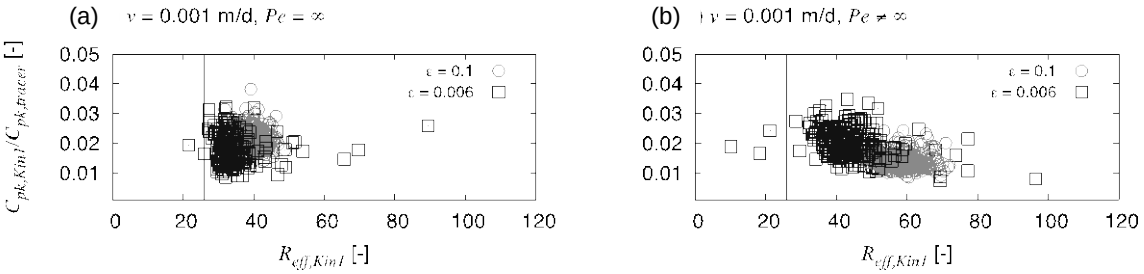

Fig. 2 *Kin1* effective retardation ratios *versus* normalized peak concentrations for each realization for infinite *Pe* (a) and finite *Pe* (b). ε are denoted by symbol (see key).

LEA ensembles (scatter plots not shown here) are centred at R_{eff} = 26 (–), showing good agreement with the expected retardation for LEA simulations. Any scatter associated with $R_{eff,LEA}$ values is associated with numerical dispersion and the time-step at which concentration is tracked as a function of time (i.e. the actual peak time may occur between measured time steps and this error, when normalized by a similar error for the tracer, gives rise to what we are referring to here as numerical scatter). The scatter associated with finite *Pe*, (right panel of Fig. 2) displays an additive effect of this numerical scatter and the increase in local dispersion. *Kin1* ensembles (Fig. 2(a)) are not centred at R_{eff} = 26 (–), where the centred values range between R_{eff} = 40 – 70 (–). The result from infinite *Pe* (Fig. 2(a)) demonstrates the later arrival time, or added tailing effect, imposed from kinetic sorption. The result from finite *Pe* (Fig. 2(b)) demonstrates the same phenomena, intensified by the effect of local dispersion. This result with respect to time is consistent with the results with respect to concentration as discussed above, the centred value of R_{eff} for finite *Pe*, *Kin1* ensembles is nearly double that of LEA ensembles. Differences in stratification are also apparent in Fig. 2, where smaller ε demonstrates less variance in R_{eff} and greater ε demonstrate more variance in R_{eff}. In other words, the normalized arrival times for more stratified domains are consistent in contrast to the less consistent arrival times with the less stratified domain. This result can also be attributed to channelling and preferential flow pathways in the stratified domain.

Measure of aquifer channelling

To investigate aquifer connectivity (often referred to as channelling or fingering), the connectivity indicator (*CI*) metric is utilized in conjunction with breakthrough times corresponding to when 50% and 5% of the mass arrives at the well. Table 2 shows statistics corresponding to the average connectivity indicator (<*CI*> (–)) and standard deviation of the connectivity indicator (σ_{CI} (–)) for varying *Pe*, and sorption scenarios.

General trends in <*CI*> include: (1) greater <*CI*> for kinetic sorption ensembles and lesser <*CI*> for LEA ensembles, (2) greater than or equal <*CI*> in ensembles including PSD and lesser or equal <*CI*> ensembles excluding PSD. This analysis also indicates <*CI*> is invariant to differences

in ε. The higher *CI* values within Table 2 signify a breakthrough curve skewed towards earlier arrival times and significant tailing. These results are consistent with the analysis presented above, where it was shown that the resulting solute peak concentration from kinetic sorption and/or PSD is retarded in time. General trends in σ_{CI} provide for greater discussion, and include: (1) greater σ_{CI} for kinetic sorption ensembles and lesser σ_{CI} for LEA ensembles, (2) much greater σ_{CI} in stratified domains (ε = 0.006) in comparison to smaller σ_{CI} in less stratified domains (ε = 0.1). σ_{CI} is invariant to differences in PSD. The most apparent of these trends is the difference in σ_{CI} with stratification (trend 2). While the mean magnitude of connectivity does not differ drastically given differences in stratification, connectivity is highly variable within the ε = 0.006 ensembles and not within the ε = 0.1 ensembles. *CI* values within stratified aquifers are as high as 3.9 (–), and as low as 1.0 (–). In the case of highly anisotropic media, multiple realizations of the ensemble are dominated by either very fast or slow flow paths, signifying σ_{CI} is a better metric for connectivity in comparison to <*CI*>. Ensembles with the greatest σ_{CI} are the *Kin1* ε = 0.006 ensembles, indicating kinetic sorption is controlling in the shape of the breakthrough curve. Finite *Pe* of these ensembles (ε = 0.006, *Kin1*) compared to infinite *Pe* also contributes to greater σ_{CI}, promoting the aforementioned finding concerning a positive feedback between kinetic sorption and PSD. A greater σ_{CI} in kinetically driven, stratified domains is physically explainable when PSD may induce movement of particles originally located in low *K* zones into high *K* channels and yield a lower effective retardation of the particle.

Table 2 *CI* statistics for each ensemble.

ε = 0.1		<*CI*>	σ_{CI}		ε = 0.006	<*CI*>	σ_{CI}
LEA	$Pe = \infty$	1.31	0.03	LEA	$Pe = \infty$	1.33	0.25
	$Pe = 1.5 \times 10^4$	1.31	0.03		$Pe = 2.5 \times 10^5$	1.50	0.25
Kin1	$Pe = \infty$	1.53	0.05	*Kin1*	$Pe = \infty$	1.48	0.32
	$Pe = 1.5 \times 10^4$	1.64	0.06		$Pe = 2.5 \times 10^5$	1.65	0.34

The probability of an individual incurring carcinogenic cancer risk was calculated (Siirila *et al*., 2012). Figure 3 shows cancer risk given a pulse source for (a) infinite *Pe* and (b) finite *Pe* to the maximally exposed individual (99th fractile of variability) at the 5th, 50th and 95th percentile of uncertainty (shown here as upper and lower bound around the 50th percentile of uncertainty). Varying v (x-axis) is presented for differences in ε for the two flow field ensembles. LEA distributions are shown in solid lines whereas *Kin1* distributions are shown in dashed lines. Remediation action levels are also plotted as horizontal lines at 10^{-6} (–).

Figure 3(a) shows the probability of risk given a pulse source and infinite *Pe* whereas Fig. 3(b) shows the probability of risk given a pulse source and finite *Pe*. For each *Pe* scenario, all ensembles are dissimilar, and dis-equilibrium conditions exist. Changes in each variable (i.e. ε, *Pe*, and sorption scenario) show sensitivity to risk. In general, upper bounds of risk increase with (1) a decrease in ε, and (2) LEA ensembles in comparison to *Kin1* ensembles. The time dependence associated with sorption kinetics diminishes the overall effect of the peak concentration (see Fig. 1), resulting in lower probabilities of cancer risk in comparison to LEA ensembles. Because mass is conserved in the simulation, the decreased peak concentration results in a smearing of the breakthrough curve tail. We previously noted the effect of kinetic sorption with $R_{eff,Kin1}$ variances is greater than the variances of $C_{pk,Kin}/C_{pk,tracer}$ and that the additive effect of PSD-kinetic sorption yield the highest change in effective retardations (Fig. 2). It is important to distinguish here that the risk simulations are directly dependent on the value of maximum concentration in the well, and do not reflect the variance in effective retardations directly.

The effect of PSD decreases both LEA and *Kin1* risk upper bound values. Differences in ε are present for finite and infinite *Pe*, consistent with the results from the $R_{eff,Disp}$ metric (Fig. 2). Here, the demonstrated parametric sensitivity is substantial, suggesting the feedbacks between processes

such as PSD and kinetic sorption are significant and should not be dismissed in risk analysis modelling or in groundwater solute transport problems.

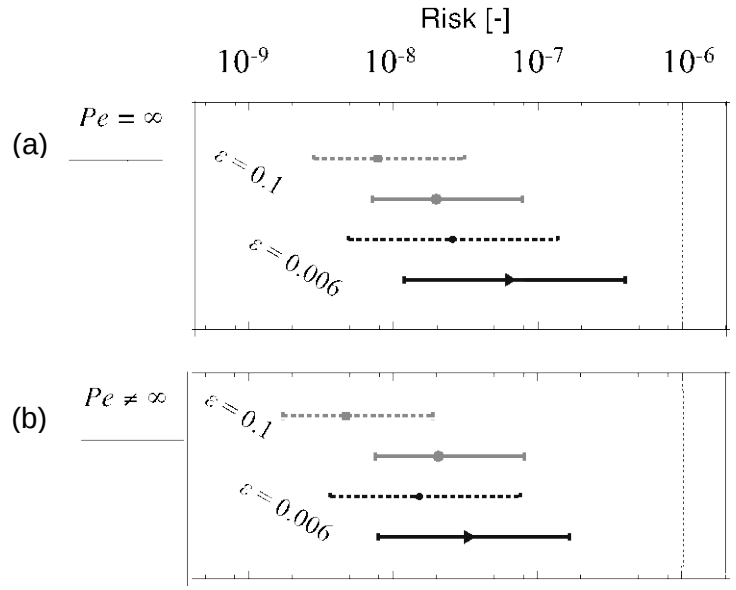

Fig. 3 Increased cancer risk for the maximally exposed individual (99th fractile of variability) for a pulse source term is shown for (a) infinite *Pe* and (b) finite *Pe*. The 99th and 5th percentiles of uncertainty are plotted as upper and lower bounds around the mean (50th percentile) for each ensemble. Varying v is also shown (x-axis) for differences in ε (see key shown in Figs 2 and 3). LEA distributions are shown in solid lines whereas *Kin1* distributions are shown in dashed lines.

CONCLUSIONS

An investigation was conducted to analyse the effect of kinetically sorbing solutes in stratified aquifers to assess realistic far-field groundwater contamination scenarios where variations in sedimentology and stratigraphy are dominant factors in determining contaminant flow and transport. An investigation of potential inter-play (positive or negative feedbacks) between multiple hydro-geologic parameters was conducted for both kinetic and LEA ensembles to assess the validity and predictability of LEA through comparisons of stochastic ensembles. Principal findings include:

(1) Parametric sensitivity to aquifer channelling is sensitive to the degree of aquifer stratification. While the mean connectivity is independent of ε, the variance in connectivity is highly dependent on ε where connectivity is highly variable stratified ensembles and not within less stratified ensembles. Either very fast (inter-connected high K zones) or slow flow (inter-connected low K zones) paths dominate realizations of highly anisotropic media. Connectivity variance is the greatest for ensembles including PSD and kinetic ensembles, further promoting the results discussed in principal finding 2.

(2) An additive, or positive feedback, between PSD and kinetic sorption was found to be a controlling process in accurately simulating solute behaviour by adding an effective tailing behaviour as high as approximately 30 times that of a LEA solute without PSD. We speculate that the effect is controlled at the high-low K interface, where the induced cell-based mixing creates particle jumps from interconnected high K regions into regions of low K and *vice versa*. The time dependence associated with kinetic sorption into and out of solution is magnified with PSD, yielding solute behaviour unlike that of equilibrium simulations when the effective retardation of kinetics is much less than R. Here we show the PSD-kinetic sorption effect retards the first moment of the plume, a second interdependence phenomenon not previously documented.

(3) In general, upper bounds of carcinogenic risk increase with a decrease in aquifer stratification. The additive PSD-kinetic sorption effect relates to a higher upper bound of risk for the continuous source and a lower upper bound of risk for the pulse source.

These results suggest small-scale mechanisms such as local dispersion and kinetic sorption are controlling of not only solute transport processes but also human health risk assessment. Implications of this study are relevant in upcoming technological challenges in contaminant transport such as CCS and other relevant human health risk assessments.

REFERENCES

Andričević, R, Daniels, J. & Jacobson, R. (1994) Radionuclide migration using a travel time transport approach and its application in risk analysis. *J. Hydrol.* 163(1–2), 125–145.

Andričević, R., & Cvetković, V. (1996) Evaluation of risk from contaminants migrating by groundwater. *Water Resour. Res.* 32(3), 611–621.

Ashby, S. & Falgout, R. (1996) A parallel multigrid preconditioned conjugate gradient algorithm for groundwater flow simulations." *Nuclear Science and Engng* 124(1), 145–159.

Bellin, A., Lawrence, A. & Rubin, Y. (2004) Models of sub-grid variability in numerical simulations of solute transport in heterogeneous porous formations, three-dimensional flow and effect of pore-scale dispersion. *Stochastic Environmental Research and Risk Assessment* 18(1), 31–38.

Benekos, I., Shoemaker, C. & Stedinger, J. (2007) Probabilistic risk and uncertainty analysis for bioremediation of four chlorinated ethenes in groundwater. *Stochastic Environmental Research and Risk Assessment* 21(4), 375–390.

Benekos, I., Shoemaker, C. A., Stedinger, J. R. & Willis, M. B. (2003) Stochastic risk analysis of bioremediation of four chlorinated ethenes incorporating age specific population variability and aquifer uncertainty. ASCE.

Bolster, D., Barahona, M., Dentz, M., Fernandez-Garcia, D., Sanchez-Vila, X., Trinchero, P., Valhondo, C. & Tartakovsky, D. M. (2009) Probabilistic risk analysis of groundwater remediation strategies. *Water Resour. Res.* 45(6), W06413.

Bolster, D. & Tartakovsky, D. (2008) Probabilistic risk analysis of building contamination. *Indoor Air-Int. J. Indoor Air Quality and Climate* 18(5), 351–364.

de Barros, F. & Rubin, Y. (2008) A risk-driven approach for subsurface site characterization. *Water Resour Res.* 44(1), W01414.

de Barros, F. P. J., Rubin, Y. & Maxwell, R. M. (2009) The concept of comparative information yield curves and its application to risk-based site characterization. *Water Resour. Res.* 45(6), W06401.

Dagan, G. & Fiori, A. (1997) The influence of pore-scale dispersion on concentration statistical moments in transport through heterogeneous aquifers. *Water Resour. Res.* 33(7), 1595–1605.

Fiori, A., Berglund, S., Cvetkovic, V. & Dagan, G. (2002) A first-order analysis of solute flux statistics in aquifers, The combined effect of pore-scale dispersion, sampling, and linear sorption kinetics. *Water Resour. Res.* 38(8), 1137.

Fiorotto, V. & Caroni, E. (2002) Solute concentration statistics in heterogeneous aquifers for finite Peclet values. *Transport in Porous Media* 48(3), 331–351.

Hassan, A. E., Andricevic, R. & Cvetkovic, V. (2001) Computational issues in the determination of solute discharge moments and implications for comparison to analytical solutions. *Adv. Water Resour.* 24(6), 607–619.

Jones, J. E. & Woodward, C. S. (2001) Newton-Krylov-multigrid solvers for large-scale, highly heterogeneous, variably saturated flow problems. *Adv. Water Resour.* 24(7), 763–774.

Knudby, C. & Carrera, J. S. (2005) On the relationship between indicators of geostatistical, flow and transport connectivity. *Adv. Water Resour.* 28(4), 405–421.

Kollet, S. J. & Maxwell, R. M. (2006) Integrated surface-groundwater flow modeling, a free-surface overland flow boundary condition in a parallel groundwater flow model. *Adv. Water Resour.* 29(7), 945–958.

Maxwell, R., Carle, S. & Tompson, A. (2008) Contamination, risk, and heterogeneity, on the effectiveness of aquifer remediation. *Environ. Geol.* 54(8), 1771–1786.

Maxwell, R. M. (2010) SLIM-FAST, A User's Manual V.4, GWMI.

Maxwell, R. M. & Kastenberg, W. E. (1999) Stochastic environmental risk analysis, an integrated methodology for predicting cancer risk from contaminated groundwater. *Stochastic Environmental Research and Risk Assessment* 13(1–2), 27–47.

Maxwell, R. M., Welty, C. & Harvey, R. W. (2007) Revisiting the Cape Cod bacteria injection experiment using a stochastic modeling approach. *ES&T* 41(15), 5548–5558.

Pickens, J., Jackson, R., Inch, K. & Merritt, W. (1981) Measurement of distribution coefficients using a radial injection dual-tracer test. *Water Resour. Res.* 17(3), 529–544.

Roberts, P. V., Goltz, M. N. & Mackay, D. M. (1986) A natural gradient experiment on solute transport in a sand aquifer, 3. Retardation estimates and mass balances for organic solutes. *Water Resour. Res.* 22(13), 2047–2058.

Siirila, E. R., Navarre-Sitchler, A. K., Maxwell, R. M. & McCray, J. E. (2012) A quantitative methodology to assess the risks to human health from CO2 leakage into groundwater. *Adv. Water Resour.* 36, 146–164.

Smalley, J. B., Minsker, B. S. & Goldberg, D. E. (2000) Risk-based in situ bioremediation design using a noisy genetic algorithm. *Water Resour. Res.* 36(10), 3043–3052.

Tartakovsky, D. M. (2007) Probabilistic risk analysis in subsurface hydrology. *Geophys. Res. Lett.* 34(5), L05404.

Tompson, A. F. B., Ababou, R. & Gelhar, L. W. (1989) Implementation of the three-dimensional turning bands random field generator. *Water Resour. Res.* 25(10), 2227–2243.